Magnetism-Dependent Transport Phenomena in Hydrogenated Graphene: From Spin-Splitting to Localization Effects

Nicolas Leconte,[†,*] David Soriano,[‡,¶] Stephan Roche,[§,∥,*] Pablo Ordejon,[⊥] Jean-Christophe Charlier,[†] and J. J. Palacios[▽]

[†]Université Catholique de Louvain, Institute of Condensed Matter and Nanosciences (IMCN), Place Croix du Sud 1 (NAPS-Boltzmann), 1348 Louvain-la-Neuve, Belgium, [‡]Departamento de Física Aplicada, Universidad de Alicante, San Vicente del Raspeig, Alicante 03690, Spain, [¶]Instituto de Ciencia de Materiales de Madrid (CSIC), Cantoblanco, Madrid, 28049, Spain, [§]CIN2 (ICN-CSIC) and Universitat Autonoma de Barcelona, Catalan Institute of Nanotechnology, Campus de la UAB, 08193 Bellaterra (Barcelona), Spain, [∥]ICREA, Institucio Catalana de Recerca i Estudis Avançats, 08010 Barcelona, Spain, [⊥]Centre de Investigació en Nanociència i Nanotecnologia, CIN2 (CSIC-ICN), Campus de la UAB, 08193 Bellaterra (Barcelona), Spain, and [▽]Departamento de Física de la Materia Condensada, Universidad Autónoma de Madrid, Cantoblanco, Madrid 28049, Spain

ABSTRACT Spin-dependent transport in hydrogenated two-dimensional graphene is explored theoretically. Adsorbed atomic hydrogen impurities can either induce a local *antiferromagnetic, ferromagnetic, or nonmagnetic* state depending on their density and relative distribution. To describe the various magnetic possibilities of hydrogenated graphene, a self-consistent Hubbard Hamiltonian, optimized by *ab initio* calculations, is first solved in the mean field approximation for small graphene cells. Then, an efficient order N Kubo transport methodology is implemented, enabling large scale simulations of functionalized graphene. Depending on the underlying intrinsic magnetic ordering of hydrogen-induced spins, remarkably different transport features are predicted for the same impurity concentration. Indeed, while the disordered nonmagnetic graphene system exhibits a transition from diffusive to localization regimes, the intrinsic ferromagnetic state exhibits unprecedented robustness toward quantum interference, maintaining, for certain resonant energies, a quasiballistic regime up to the micrometer scale. Consequently, low temperature transport measurements could unveil the presence of a magnetic state in weakly hydrogenated graphene.

KEYWORDS: disordered graphene · quantum transport · metal−insulator transition · ballistic transport · numerical simulation · hydrogenation · graphene spintronics

The peculiar low energy electronic excitations in graphene[1] trigger unusual transport properties[2] and drive promising (and flourishing) carbon-based technologies.[3−5] On the other hand, magnetic nanostructures based on carbon, are particularly attractive for future applications in spintronics.[6−9] A few experiments suggest the existence of magnetic states in graphite[10,11] and graphene,[12] but to date, unambiguous evidence of intrinsic magnetism in graphene remains elusive.[13] One possible reason related to the difficulty of detecting magnetic states graphene and carbon-based nanostructures lies on the fact that hydrocarbons of high spin are known to be highly reactive, avid to be passivated by surrounding species.[14] On more fundamental grounds, the electronic ground state of semimetallic graphene is close to an interaction-driven insulating antiferromagnetic state.[15] Indeed, these underlying antiferromagnetic correlations prevent the magnetic moments or spin textures, even if they develop, from ordering in a collective ferromagnetic state, thus hindering any manifestation in standard magnetization measurements.

Structural disorder such as monovacancies or sp^3-type defects have been theoretically predicted to induce local spin polarization[16−18] and, in certain circumstances, promote long-range magnetic ordering. Hydrogen functionalization is, for instance, a possible way to tune electronic properties and magnetism in graphene. Attempts to turn the carbon sheet into an insulating material by hydrogenation (graphane) have recently been reported,[19−21] but spin-dependent features remain to be explored in this context. In general, the connection between possible underlying defect-induced magnetic order in graphene and its transport signature is largely unexplored. In this paper, different transport properties are found to directly depend on the nature of the underlying magnetic state of hydrogenated graphene, as predicted by means of a combined approach of a self-consistent spin-dependent Hubbard Hamiltonian with a computationally order N transport method.

* Address correspondence to nicolas.leconte@uclouvain.be, stephan.roche@icn.cat.

Received for review February 11, 2011 and accepted April 6, 2011.

Published online April 06, 2011
10.1021/nn200558d

Disordered antiferromagnetic and nonmagnetic states are demonstrated to be sensitive to localization effects in the low temperature regime and high defect density, whereas a complete suppression of quantum interferences is observed in the ferromagnetic state for similar hydrogen concentrations.

RESULTS AND DISCUSSION

Electronic structure calculations of hydrogenated graphene supercells are performed using *ab initio* techniques, together with a single π-orbital first-neighbor tight-binding model, where the Coulomb interaction is treated in the mean field approximation by means of a Hubbard-like interaction (see Methods). The chemisorption of a hydrogen (H) atom on top of a carbon (C) atom changes the local sp^2-configuration and can be simulated in the tight-binding approach by removing the functionalized carbon site.[22] This broken sublattice symmetry gives rise to resonances near the Dirac point[23] which spin-polarize when the Coulomb repulsion is included in the calculation. The resulting magnetic moments are located over the surrounding graphene with a varying degree of localization which depends on the relative position with respect to the edges of graphene or to other impurities.

In the following, systems containing two vacancies (two hydrogen atoms) per supercell, are considered to enable the correlation of the magnetic moments of both defects. Such a correlation eventually leads to a local magnetic ordering which can be either *antiferromagnetic* if the magnetic moments are counter-polarized (Figure 1, right panel) or *ferromagnetic* if they are copolarized (Figure 1, left panel). The first investigated magnetic correlation consists in removing two lattice sites in each supercell, one on each sublattice. The total spin (S) of the ground state of a bipartite lattice is obtained by the straightforward application of Lieb's theorem[24] which relates the total spin of a bipartite lattice to the difference between sublattice sites ($2S = N_A - N_B$). As $N_A - N_B = 0$ for the AB case, Lieb's theorem predicts either a nonmagnetic (NM) or an antiferromagnetic ground state (AF-AB from hereon), both with $S = 0$. To explore the effect of varying the hydrogen concentration, different supercell sizes are investigated (see insets in Figure 1). The distance between hydrogen atoms was decreased while reducing the supercell size.

Lieb's theorem also predicts a ferromagnetic ground state ($S \neq 0$) when the two sublattices present an uncompensated hydrogenation. Zhou *et al.*[25] suggested a semiconducting graphene with one sublattice fully hydrogenated (also known as *graphone*). Although the selective hydrogenation of the A (or B) sublattice of a graphene sample is a challenging task, disorder-driven hydrogenation such as ripples in suspended graphene or surface effects in deposited

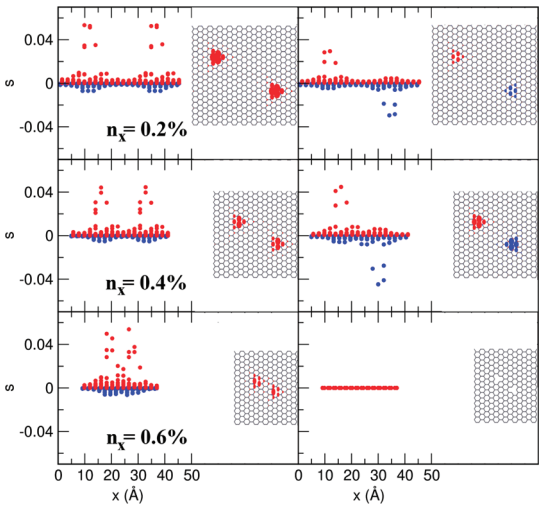

Figure 1. Local spin (s) *versus* the distance on the *x*-axis (*x*) for vacancy (or hydrogen) concentrations n_x = 0.2, 0.4, and 0.6% in the ferromagnetic (left panel) and antiferromagnetic (right panel) cases. Red (blue) dots correspond to spin up (down) electrons. Insets: Top-view projections of the local spin densities.

samples could give rise to slightly uncompensated lattices, favoring a ferromagnetic ground state. To explore possible intrinsic ferromagnetic transport responses, we therefore investigate theoretically the case of totally uncompensated functionalization (AA or BB), where both chemisorbed hydrogen atoms lie on the same sublattice in the supercell (referred as F-AA hereon). Figure 1 illustrates the local spin density for the situation of antiferromagnetic (right panel) and ferromagnetic (left panel) couplings with various hydrogen concentrations. An important observation is the disappearance of the spin density for the AF-AB case for hydrogen densities $n_x \geq 0.6\%$, which contrasts to the robustness of the intrinsic ferromagnetic case.

The transport properties of disordered/hydrogenated graphene are computed using an efficient order N Kubo-Greenwood transport method (see Methods). Figure 2 (left frame) illustrates how the random distribution of pairs is built from the initial supercells.

For low hydrogen concentrations ($n_x < 0.6\%$), where local spin densities survive even for the AF-AB, localization effects appear to be limited within the reach of calculation times (Figure 3, left panel, inset). We focus on the higher concentration limit ($n_x = 0.8\%$) in which the local spin has been suppressed yielding a global nonmagnetic state. Figure 3 (left frame) presents $D_\uparrow(E,t)$ for $n_x = 0.8\%$ at three selected energies. These diffusion coefficients are clearly reaching a saturation regime after a few hundreds of femtoseconds. Then, they exhibit a strong logarithmic decay which is an unambiguous fingerprint of weak localization effects.[26] The behavior of the corresponding elastic mean free path ℓ_e is illustrated in Figure 4 (inset). Away from the Dirac point, $\ell_e \approx 1/n_x$ as expected from a simple Fermi Golden rule. At lower energies, ℓ_e fluctuates within

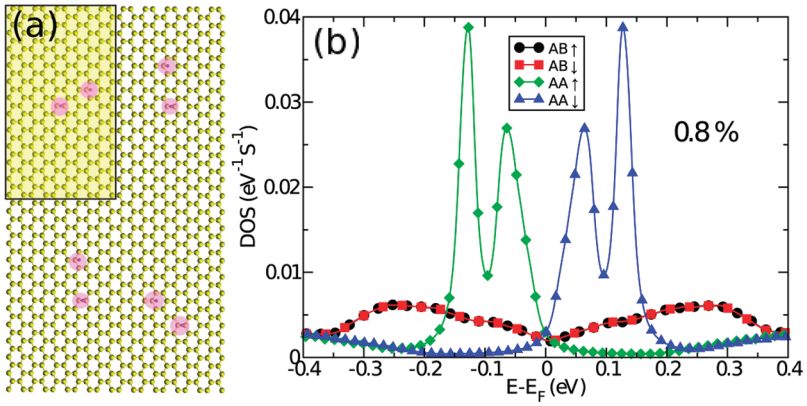

Figure 2. (a) Schematic (and reduced) view of an hydrogenated magnetic graphene (the original supercell is shaded by a yellow rectangle). Each supercell contains one pink-shaded vacancy pair. (b) DOS plots for both the AB and AA configurations for n_x = 0.8%.

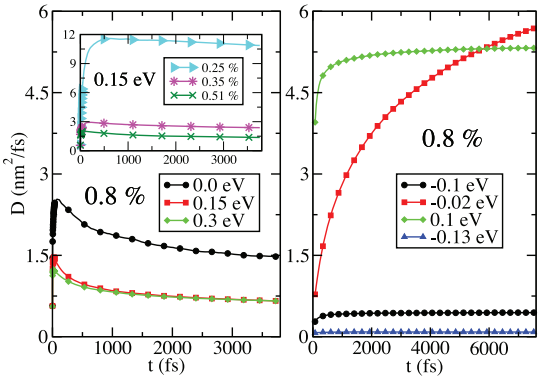

Figure 3. Time-dependent diffusion coefficients (spin up channel) for selected energies (see legends) for a n_x = 0.8% hydrogen impurity concentration, in the NM (left frame) and F-AA (right frame) configurations. Inset in the left frame gives the diffusion coefficients at 0.15 eV for lower concentrations in the AB case.

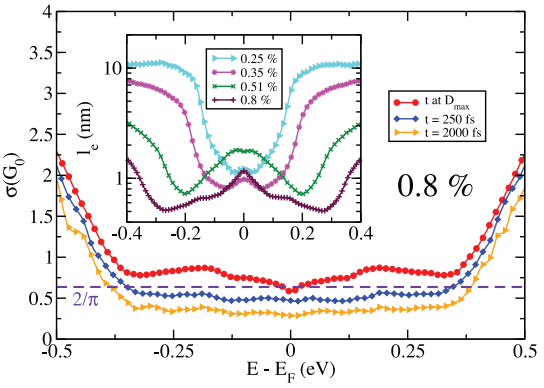

Figure 4. Main frame: Kubo conductivities for the NM magnetic state with n_x = 0.8% hydrogen impurities. The values at D_{max} (extracted at $t \approx 50$ fs) gives access to the Drude conductivity, whereas values at longer elapsed times clearly encompass localization effects. The theoretical limit for Drude conductivity ($4e^2/h\pi$) is represented by the horizontal dashed line. Inset: Spin-degenerate elastic mean free path for various hydrogen concentrations.

1−2 nm, presenting a weak hydrogen-concentration dependence.

Figure 4 (mainframe) displays both the corresponding Drude and Kubo conductivities. The latter are evaluated at larger elapsed times when quantum interferences cannot be neglected. Note that the total Drude conductivity always remains higher than $2G_0/\pi = 4e^2/\pi h$ (G_0 the conductance quantum) in full agreement with the analytical results derived from the self-consistent Born approximation.[27] The increase of the conductivity at the Dirac point with respect to the clean limit value $2G_0/\pi$ has also been theoretically established for Dirac (single-valley) electrons and many types of disorder, being actually observed in most graphene samples.[28] This can be explained by intravalley scattering (dominant over intervalley one) which is induced either by intrinsic (ripples) or extrinsic disorder (charged impurities) always accidentally present in most samples.[29] On the contrary, as soon as quantum interferences come into play in our intentionally disordered systems, $\sigma_{\uparrow,\downarrow}(E,t)$ becomes lower than its semiclassical limit, pinpointing the transition to a weak localization regime, as illustrated in Figure 4 (mainframe) for two elapsed times t = 250 fs and t = 2000 fs. From the computed electronic mean free path ℓ_e, the corresponding localization length can be estimated using the relationship $\xi(E) = \ell_e \exp(\pi\sigma_{Drude}/2G_0)$.[26] Close to the charge neutrality point, localization lengths are predicted to be in the range of *ca.* 8−15 nm for defect densities between 0.25% and 0.8%. Note that this transition to a weak localization regime has been overlooked in recent works where similar models predict conductivity values well above $4e^2/\pi h$[30] at the Dirac point. Our result is, in addition, consistent with experimental findings.[19]

Figure 3 (right frame) presents $D_\uparrow(E,t)$ for the F−AA case. Conversely to the NM case, for identical defect densities, the establishment of a diffusive regime at much longer times pinpoints a much weaker effect from backscattering. Additionally, the saturation of $D_\uparrow(E,t)$ to its maximum value is not observed to be followed by a logarithmic decay as expected in the

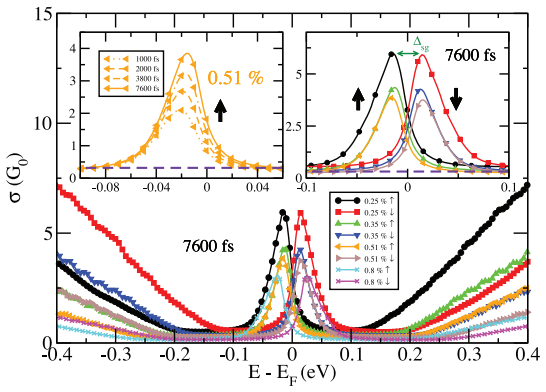

Figure 5. Main frame: Kubo conductivities for the F−AA magnetic state for different concentrations of hydrogen impurities and for up and down spin configurations, for an elapsed time of t = 7600 fs. Left inset: time-dependent evolution of $\sigma_\uparrow(E)$ for n_x = 0.51% close to the resonance energy $\varepsilon_\uparrow^r \approx -15$ meV. Right inset: zoom in on the spin-split gap Δ_{sg} (same hydrogen concentrations as in the mainframe). Dashed horizontal lines give $2e^2/\pi h$.

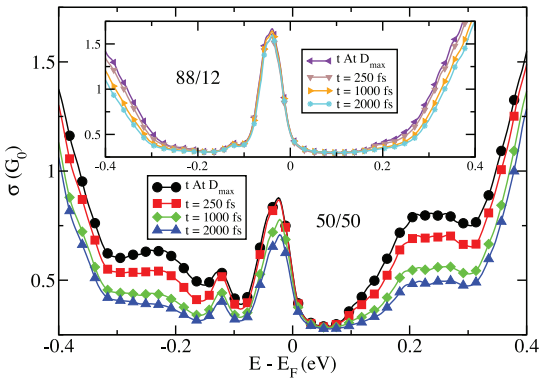

Figure 6. Main frame: Time dependent Kubo conductivities (up channel) for 50% of AA pairs and 50% of AB pairs in the supercell. Inset: 88% of AA pairs and 12% of AB pairs. Down channel (not shown) is symmetric over the Fermi energy.

presence of weak localization effects. Figure 5 presents the Drude conductivities for the intrinsic ferromagnetic situation F−AA computed at t = 7600 fs (for n_x = 0.8%). First, in sharp contrast to the nonmagnetic case, a strong spin-splitting is observed around the charge neutrality point (mainframe), as manifested by the two separated (resonant) peaks for up [$\sigma_\uparrow(E)$] and down spin [$\sigma_\downarrow(E)$] populations, occurring respectively at energies $\varepsilon_\uparrow^r \simeq -15$ meV ($\varepsilon_\downarrow^r \simeq +15$ meV). The spin gap $\Delta_{sg} = |\varepsilon_\uparrow^r - \varepsilon_\downarrow^r|$ ranges within [25,30]meV for n_x = 0.25−0.8% (see Figure 5, right inset) and originates from the strong local Coulomb interaction between the two spin-polarized states near the impurities. On the other hand, the total conductivity is found to decay with hydrogen concentration but saturates at $4e^2/\pi h$ for energies away from the resonant peaks. Such a saturation is concomitant to the robust diffusive regime established after an initial ballistic extension of the wavepackets, but unaffected by further quantum interferences (as calculated for four energies in the right frame of Figure 3). The DOS peaks in Figure 2 (right panel) are part of this diffusive plateau. In Figure 5, left inset, $\sigma_\uparrow(E,t)$ for $n_x \simeq 0.5\%$ is depicted for increasing elapsed times (similar trend is found for $n_x \simeq 0.8\%$). Surprisingly, in the vicinity of $\varepsilon_{\downarrow,\uparrow}^r$, the conductivities are seen to increase with time without saturation (up to our computational limits). This behavior is not a numerical artifact, but rather illustrates the absence of backscattering, manifesting a robust quasi-ballistic regime and suggesting the contribution of Klein tunneling process.[31]

The comparison between the NM and F−AA cases for the same hydrogen concentration is therefore particularly striking. The strong reduction of backscattering and complete suppression of quantum interferences for the F-AA case (in which the B-sites sublattice remains free of any defects) partly stems from a preserved chiral symmetry of the Hamiltonian.[27] The robustness of transport in such a situation is also likely related to pseudospin effects which trigger Klein tunneling and weak antilocalization phenomena.[31,32] Additionally, this specific symmetry resulting in full imbalance between functionalized A sites and defect free B sites, also roots the establishment of strong ferromagnetism. In brief, one of the most interesting findings is thus the connection between ferromagnetic order and absence of localization effects.

Finally, two intermediate situations containing respectively 50% (88%) of AA vacancies and 50% (12%) of AB vacancies are studied in Figure 6. For the 50/50 case, notable localization effects set in while keeping a nonuniform conductivity profile in the whole of the energy spectrum, in contrast with the fully balanced AB case in Figure 4.

CONCLUSIONS

Intrinsic ordered magnetic states are demonstrated to exhibit a very specific transport signature in large-size hydrogenated graphene in the low temperature limit. An intrinsic ferromagnetic state will take place in the case of exclusive functionalization of one out of the two sublattices. In this situation, the material would be strongly (anomalously) robust to localization phenomena (up to hydrogen densities $n_x \leq 1\%$), either presenting a saturation of the low-temperature conductivity to its Drude value, or a quasiballistic motion at some resonant energies. In striking contrast, for similar defect densities, a disorder antiferromagnetic and a nonmagnetic state will suffer from quantum interferences (beyond the diffusive regime) and localization effects will manifest in the low temperature regime, for instance through a variable range hopping behavior (as also observed in other types of damaged graphene[33]). These theoretical predictions provide a possible guidance for further experimental transport measurements and scrutiny of magnetism in hydrogenated graphene.[34] One finally remarks that other types of functionalization (such as

adsorbed NO_2 gases or fluorination) could provide alternative routes to induce strong spin-polarized impurity states and high temperature magnetic order in graphene.[35−37]

METHODS

Electronic structure calculations of hydrogenated graphene supercells are performed using *ab initio* techniques within the local spin density approximation (LSDA),[38] together with a single π-orbital first-neighbor tight-binding model, where the Coulomb interaction is treated in the mean field approximation by means of a Hubbard-like interaction U. Both approaches have already been successfully employed to investigate nanoribbons and nanographenes,[39−41] typically assuming a full passivation by H of the edge σ-bonds. The spin-dependent Hamiltonian of hydrogenated graphene reads $\mathcal{H} = t\sum_{\langle i,j\rangle,\sigma} c^{\dagger}_{i,\sigma}c_{j,\sigma} + U\sum_i n_{i,\uparrow}\langle n_{i,\downarrow}\rangle + n_{i,\downarrow}\langle n_{i,\uparrow}\rangle$, where t is the first-neighbor hopping term, $c^{\dagger}_{i,\sigma}$ ($c_{j,\sigma}$) is the creation (annihilation) operator of an electron in the lattice site i (j) with spin σ, U is the on-site Coulomb repulsion[42] and $n_{i,\downarrow}$, $n_{i,\uparrow}$ are the self-consistent occupation numbers for spin-down and spin-up electrons, respectively. The typical U/t ratio used to model graphene-based systems using the Hubbard model ranges between 0.9 and 1.3.[42]

The transport properties of disordered/hydrogenated graphene are computed using an efficient order N Kubo-Greenwood transport method.[33,43,44] From the time-dependent analysis of the wavepacket dynamics, conduction regimes and transport length scales such as the mean free path are extracted. The spin-dependent Kubo conductivity (at zero temperature and zero frequency) reads $\sigma_{\uparrow,\downarrow}(E,t) = (e^2/2)\mathrm{Tr}[\delta_{\uparrow,\downarrow}(E - \hat{H})]D_{\uparrow,\downarrow}(E,t)$ with $\mathrm{Tr}[\delta_{\uparrow,\downarrow}(E - \hat{H})/S]$ the spin-dependent densities of states per surface unit at Fermi energy E. At a fixed energy, $\sigma_{\uparrow,\downarrow}(E,t)$ reach their maximal values at the same time as $D_{\uparrow,\downarrow}(E,t)$ ($D^{\max}_{\uparrow,\downarrow}$) allowing the estimation of the spin-dependent Drude conductivities $\sigma^{\mathrm{Drude}}_{\uparrow,\downarrow}(E) = (e^2/2)\mathrm{Tr}[\delta_{\uparrow,\downarrow}(E - \hat{H})]D^{\max}_{\uparrow,\downarrow}(E))$, that account for the disorder effects on the density of states. The maximum value $D^{\max}_{\uparrow,\downarrow}(E)$ of the diffusion coefficient also gives a numerical value to the elastic mean free path, since $\ell_e = D_{\max}/2vF$ (where $v_F = 10^6$ ms^{-1}). At longer time, $D_{\uparrow,\downarrow}(E,t)$ can exhibit a logarithmic decay in the presence of quantum interferences. The corresponding Kubo conductivity is thus reduced compared to its Drude value, as long as quantum coherence is maintained.

Acknowledgment. D.S., J.J.P., and P.O. acknowledge financial support from Spanish MICINN under Grants FIS2010-21883-C02-02 and CONSOLIDER CSD2007-00010 (D.S. and J.J.P.) and FIS2009-12721-C04-1 and CONSOLIDER CSD2007-050 (P.O.). D.S. acknowledges Ph.D. Grant Program from CSIC and the Unidad Asociada of the Universidad de Alicante. This work is directly connected to research contracts with the FNRS of Belgium, to the Belgian Program on Interuniversity Attraction Poles (PAI6), to the ARC sponsored by the Communauté Française de Belgique, to the ETSF e-I3 project (Grant No. 211956), and to the NANOSIM-GRAPHENE project (ANR-09-NANO-016-01) of ANR/P3N2009. Computational resources were provided by the CISM of the Université Catholique de Louvain.

REFERENCES AND NOTES

1. Geim, A. K.; Novoselov, K. S. The Rise of Graphene. *Nat. Mat.* **2007,** *6*, 183–191.
2. Neto, A. H. C.; Guinea, F.; Peres, N. M. R.; Novoselov, K. S.; Geim, A. K. The Electronic Properties of Graphene. *Rev. Mod. Phys.* **2009,** *81*, 109–162.
3. Schwierz, F. Graphene Transistors. *Nat. Nanotechnol.* **2010,** *5*, 487–496.
4. Xia, F.; Farmer, D. B.; Lin, Y.; Avouris, P. Graphene Field-Effect Transistors with High On/Off Current Ratio and Large Transport Band Gap at Room Temperature. *Nano Lett.* **2010,** *10*, 715–718.
5. Lin, Y. M.; Jenkins, K. A.; Valdes-Garcia, A.; Small, J. P.; Farmer, D. B.; Avouris, P. Operation of Graphene Transistors at Gigahertz Frequencies. *Nano Lett.* **2008,** *9*, 422–426.
6. Yazyev, O. Emergence of Magnetism in Graphene Materials and Nanostructures. *Rep. Prog. Phys.* **2010,** 056501.
7. Banhart, F.; Kotakoski, J.; Krasheninnikov, A. V. Structural Defects in Graphene. *ACS Nano* **2011,** 250–254.
8. Maassen, J.; Ji, W.; Guo, H. Graphene Spintronics: The Role of Ferromagnetic Electrodes. *Nano Lett.* **2011,** 323–349.
9. Singh, A. K.; Yakobson, B. I. Electronics and Magnetism of Patterned Graphene Nanoroads. *Nano Lett.* **2009,** *9*, 1540–1543.
10. Esquinazi, P.; Spemann, D.; Höhne, R.; Setzer, A.; Han, K. H.; Butz, T. Induced Magnetic Ordering by Proton Irradiation in Graphite. *Phys. Rev. Lett.* **2003,** *91*, 227201.
11. Ohldag, H.; Esquinazi, P.; Arenholz, E.; Spemann, D.; Rothermel, M.; Setzer, A.; Butz, T. The Role of Hydrogen in Room-Temperature Ferromagnetism at Graphite Surfaces. *New J. Phys.* **2010,** 123012.
12. Wang, Y.; Huang, Y.; Song, Y.; Zhang, X.; Ma, Y.; Liang, J.; Chen, Y. Room-Temperature Ferromagnetism of Graphene. *Nano Lett.* **2008,** *9*, 220–224.
13. Sepioni, M.; Nair, R. R.; Rablen, S.; Narayanan, J.; Tuna, F.; Winpenny, R.; Geim, A. K.; Grigorieva, I. V. Limits on Intrinsic Magnetism in Graphene. *Phys. Rev. Lett.* **2010,** *105*, 207205.
14. Makarova, T.; Palacio, F. *Carbon Based Magnetism: An Overview of the Magnetism of Metal Free Carbon-Based Compounds and Materials*; Elsevier Science and Technology, 2006.
15. Sorella, S.; Tosatti, E. Semi-metal-insulator Transition of the Hubbard Model in the Honeycomb Lattice. *Europhys. Lett.* **1992,** *19*, 699.
16. Yazyev, O. V.; Helm, L. Defect-Induced Magnetism in Graphene. *Phys. Rev. B* **2007,** *75*, 125408.
17. Palacios, J. J.; Fernández-Rossier, J.; Brey, L. Vacancy-Induced Magnetism in Graphene and Graphene Ribbons. *Phys. Rev. B* **2008,** *77*, 195428.
18. Dubois, S. M. M.; Zanolli, Z.; Declerck, X.; Charlier, J.-C. Electronic Properties and Quantum Transport in Graphene-Based Nanostructures. *Eur. Phys. J. B* **2009,** *72*, 1.24.
19. Elias, D. C.; Nair, R. R.; Mohiuddin, T. M. G.; Morozov, S. V.; Blake, P.; Halsall, M. P.; Ferrari, A. C.; Boukhvalov, D. W.; Katsnelson, M. I.; Geim, A. K.; *et al.* Control of Graphene's Properties by Reversible Hydrogenation: Evidence for Graphane. *Science* **2009,** *323*, 610.
20. Balog, R.; Jørgensen, B.; Nilsson, L.; Andersen, M.; Rienks, E.; Bianchi, M.; Fanetti, M.; Lægsgaard, E.; Baraldi, A.; Lizzit, S.; *et al.* Bandgap Opening in Graphene Induced by Patterned Hydrogen Adsorption. *Nat. Mater.* **2010,** *9*, 315.
21. Bostwick, A.; McChesney, J. L.; Emtsev, K. V.; Seyller, T.; Horn, K.; Kevan, S. D.; Rotenberg, E. Quasiparticle Transformation During a Metal-Insulator Transition in Graphene. *Phys. Rev. Lett.* **2009,** *103*, 56404.
22. Soriano, D.; Muñoz-Rojas, F.; Fernández-Rossier, J.; Palacios, J. J. Hydrogenated Graphene Nanoribbons for Spintronics. *Phys. Rev. B* **2010,** *81*, 165409.
23. Peres, N. M. R.; Guinea, F.; Neto, A. H. C. Electronic Properties of Disordered Two- Dimensional Carbon. *Phys. Rev. B* **2006,** *73*, 125411.
24. Lieb, E. H. Two Theorems on the Hubbard Model. *Phys. Rev. Lett.* **1989,** *62*, 1201–1204.
25. Zhou, J.; Wang, Q.; Sun, Q.; Chen, X. S.; Kawazoe, Y.; Jena, P. Ferromagnetism in Semihydrogenated Graphene Sheet. *Nano Lett.* **2009,** *9*, 3867–3870.
26. Akkermans, E.; Montambaux, G. *Mesoscopic Physics of Electrons and Photons*; Cambridge University Press: New York, 2007.

27. Ostrovsky, P. M.; Gornyi, I. V.; Mirlin, A. D. Electron Transport in Disordered Graphene. *Phys. Rev. B* **2006,** *74*, 235443.
28. Sarma, S. D.; Adam, S.; Hwang, E. H.; Rossi, E. Electronic Transport in Two Dimensional Graphene. *Rev. Mod. Phys.* **2011**in press.
29. Palacios, J. J. Origin of the Quasi-universality of the Minimal Conductivity of Graphene. *Phys. Rev. B* **2010,** *82*, 165439.
30. Wehling, T. O.; Yuan, S.; Lichtenstein, A. I.; Geim, K. A.; Katsnelson, M. I. Resonant Scattering by Realistic Impurities in Graphene. *Phys. Rev. Lett.* **2010,** *105*, 056802.
31. Katsnelson, M. I.; Novoselov, K. S.; Geim, A. K. Chiral Tunnelling and the Klein Paradox in Graphene. *Nat. Phys.* **2006,** *2*, 620.
32. Morpurgo, A. F.; Guinea, F. Intervalley Scattering, Long-Range Disorder, and Effective Time-Reversal Symmetry Breaking in Graphene. *Phys. Rev. Lett.* **2006,** *97*, 196804.
33. Leconte, N.; Moser, J.; Ordejon, P.; Tao, H. H.; Lherbier, A.; Bachtold, A.; Alsina, F.; Torres, C. M. S.; Charlier, J.-C.; Roche, S. Damaging Graphene with Ozone Treatment: A Chemically Tunable Metal-Insulator Transition. *ACS Nano* **2010,** *4*, 4033–4038.
34. Jaiswal, M.; Lim, C. H. Y. X.; Bao, Q. L.; Toh, C. T.; Loh, K. P.; Ozyilmaz, B. Controlled Hydrogenation of Graphene Sheets and Nanoribbons. *ACS Nano.* **2011,** *5*, 888–896.
35. Loh, K.; Bao, Q.; Ang, P. Q.; Yang, J. The Chemistry of Graphene. *J. Mater. Chem.* **2010,** 2277–2289.
36. Wehling, T. O.; Novoselov, K. S.; Morozov, S. V.; Vdovin, E. E.; Katsnelson, M. I.; Geim, A. K.; Lichtenstein, A. I. Molecular Doping of Graphene. *Nano Lett.* **2008,** *8*, 173–177.
37. Ewels, C. P.; Lier, G. V.; Charlier, J.-C.; Heggie, M. I.; Briddon, P. R. Pattern Formation on Carbon Nanotube Surfaces. *Phys. Rev. Lett.* **2006,** *96*, 216103.
38. The one-orbital mean-field Hubbard model have been favorably compared with density functional theory (DFT) calculations using the CRYSTAL *ab initio* package. To do so, a supercell with a single H atom adsorbed onto the graphene lattice (corresponding to the n_x = 0.3% case) was used for the comparison. The atomic structure of the chemisorbed hydrogen has been relaxed locally to obtain the typical sp^3-configuration. First-principles calculations have been performed using the Perdew–Burke–Ernzerhof (PBE) exchange-correlation functional. For the carbon (C) atoms, a valence basis set (2s,2p) has been used with the core electrons replaced by a pseudopotential, while a STO-3G basis set was chosen to describe the 1s orbital of the hydrogen (H) atoms.
39. Son, Y. W.; Cohen, M. L.; Louie, S. G. Energy Gaps in Graphene Nanoribbons. *Phys. Rev. Lett.* **2006,** *97*, 216803.
40. Fernández-Rossier, J.; Palacios, J. J. Magnetism in Graphene Nanoislands. *Phys. Rev. Lett.* **2007,** *99*, 177204.
41. Hod, O.; Barone, V.; Scuseria, G. E. Half-Metallic Graphene Nanodots: A Comprehensive First-Principles Theoretical Study. *Phys. Rev. B* **2008,** *77*, 035411.
42. Pisani, L.; Chan, J. A.; Montanari, B.; Harrison, N. M. Electronic Structure and Magnetic Properties of Graphitic Ribbons. *Phys. Rev. B* **2007,** *75*, 064418.
43. Roche, S. Quantum Transport by Means of O (N) Real-Space Methods. *Phys. Rev. B* **1999,** *59*, 2284.
44. Ishii, H.; Triozon, F.; Kobayashi, N.; Hirose, K.; Roche, S. Charge Transport in Carbon Nanotubes Based Materials: A Kubo-Greenwood Computational Approach. *C. R. Phys.* **2009,** *10*, 283–296.